J Appl Electrochem (2016) 46:841–849
DOI 10.1007/s10800-016-0934-4

RESEARCH ARTICLE

In situ growth of RuO_2–TiO_2 catalyst with flower-like morphologies on the Ti substrate as a binder-free integrated anode for chlorine evolution

Kun Xiong[1] · Lishan Peng[1] · Yao Wang[1] · Linghui Liu[1] · Zihua Deng[1] · Li Li[1] · Zidong Wei[1]

Received: 3 December 2015 / Accepted: 21 January 2016 / Published online: 29 January 2016

Abstract We report a facile and controllable approach to design anodic catalysts with different surface morphologies. The RuO_2–TiO_2 anodes are directly grown in situ on the surface of Ti substrate under certain hydrothermal conditions. X-ray diffraction, field-emission scanning electron microscopy, energy dispersive X-ray spectra, cyclic voltammetry, and linear scanning voltammetry (LSV) were used to scrutinize the electrodes and the electrochemical activity. The experimental results indicate that solvothermal crystallization in the presence of hydrochloric acid plays a critical role in regulating the catalyst size and microstructure during the nucleation and growth process of RuO_2–TiO_2. The designed RuO_2–TiO_2/Ti anode with a nano-flowerlike structure displays significantly enhanced activity toward anodic chlorine evolution reaction (CER) compared to the other two morphology anodes. Such excellent performance of RuO_2–TiO_2/Ti is explained in terms of the small charge transfer resistance and the unique surface structure with more active sites to be utilized during CER.

Graphical abstract

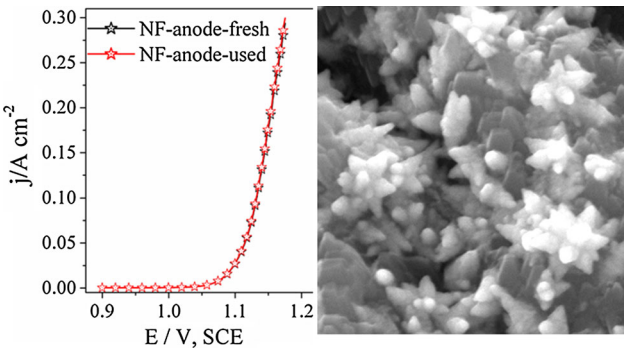

Keywords Ruthenium oxide · Titanium oxide · Hydrothermal synthesis · Morphology · Chlorine evolution reaction

1 Introduction

The chlor-alkali electrolysis is one of the most important bulk products in modern electrochemistry applications [1, 2]. In this process, the concentrated aqueous NaCl solutions are electro-catalyzed producing Cl_2 at the anode for the production of polymers, pharmaceuticals, and disinfectants, while hydrogen production at the cathode is a clean, environmentally friendly resource and considered as one of the most promising candidates for replacing fossil fuels in the future [3–5].

Since dimensionally stable anodes (DSA) were applied to replace graphite anodes in the chlor-alkali electrolysis by H. B. Beer in 1965 [6], they brought a revolution in the electrochemical technology. Such innovation in turn

✉ Zidong Wei
zdwei@cqu.edu.cn

[1] Chongqing Key Laboratory of Chemical Process for Clean Energy and Resource Utilization, College of Chemistry and Chemical Engineering, Chongqing University, Chongqing 400044, China

promotes the development of fundamental research, such as the design of electrodes and understanding of their fundamental properties of electrocatalysis by using analysis technologies and density functional theory calculations [7–17]. Commonly, employed as electrode materials, typical ruthenium-based oxides are routinely prepared by oxidative pyrolysis or sol–gel techniques [7–10, 18–20], which proceed via several coating and calcination steps until the desired catalyst loading is achieved. Therefore, the phenomenon of the growth and aggregation of active species is always accompanied by the formation of typical mud-cracks for coatings due to the thermally induced internal stresses [21, 22].

Despite the lack of consensus regarding the chlorine evolution reaction (CER) mechanisms [23–25], the oxidation and adsorption of Cl^- occurs on the surface of RuO_2 species. Thus, controlling the surface morphology and dispersion of the catalyst is considered greatly promising in the exposure of more RuO_2 active sites to the reactive two-phase zone (solid/liquid interface). With the rapid progress of nanoscience and technology in the last few years, nanomaterials have attracted much attention in the fields of chemistry, energy and electronics because they possess high surface area and some unique properties, which are significantly different from those bulk materials. Hydrothermal synthesis is yet one class of simple and effective strategies to design nanoscale controllable catalysts. The variation of hydrothermal conditions such as temperature, pH, solvent, concentration and molar ratio of reactant imparts tunable morphologies and nano/micro-structures [26–28]. Such synthesis of mesocrystalline rutile TiO_2 nanorod arrays on Ti substrate via hydrothermal condition exhibited excellent quasi-omnidirectional antireflection performance [29]. Through a facile hydrothermal reaction, a special porous $Zn_2Ti_3O_8$ nanorods architecture could be also successfully fabricated, which showed enhanced photocatalytic activity for overall water splitting, coupled with RuO_2 as co-catalysts [30]. These reports provide us a hint as to how electrodes with different morphologies might be successfully designed by hydrothermal synthesis, in which the precursors of metal salt will hydrolyze with water at the water/substrate interface, resulting in the formation of a crystal nucleus on the substrate. After the formation of the first nanocrystalline layer, the deposition films are gradually formed with continuous hydrolysis and subsequent growth-crystallization. These films with three-dimensional structure obtained by controlling the hydrothermal conditions can increase the dispersion of the catalyst, promoting the exposure of more RuO_2 active sites to the reactive two-phase zone (solid/liquid interface), compared to the conventional planar catalyst films.

Herein, we try to utilize this strategy to fabricate a uniform Ru-based catalyst toward electrocatalytic chlorine evolution, albeit no similar reports have thus far appeared in the literature. In this process, the Ti substrate could be etched by the HCl aqueous solution to obtain titanium precursor during the hydrothermal condition. The hydrolysis of titanium and ruthenium precursors is accompanied by the formation of nucleation, which is influenced by the presence of the Cl^-. Thus, the surface morphology of RuO_2–TiO_2/Ti anode could be effectively controlled. After annealing treatment, the obtained RuO_2–TiO_2/Ti anode with nano-flowerlike structure exhibit superior electrocatalytic activity and stability for CER than that of the anode prepared via the conventional thermal decomposition method.

2 Experimental

2.1 Materials synthesis

In a typical synthesis, a Ti substrate (50.0 mm × 10.0 mm × 0.25 mm) was cleaned initially by sonication in acetone, distilled water, and then etched in 18 wt% HCl at 358 K for 15 min to remove the oxide layer on the surface. The Ti substrate was placed against the wall of a Teflon liner at a certain angle, with the surface of interest facing down. About 1 cm^2 of the Ti substrate was immersed into 10 mL aqueous solution containing 5 mmol L^{-1} $RuCl_3$ and HCl with different concentrations (0.5, 1.0, and 3.0 wt%, respectively) in a Teflon-lined stainless-steel autoclave (50 mL). The autoclave was sealed and heated at 473 K for 15 h. After the hydrothermal treatment, the samples were completely washed with distilled water and dried. Finally, the samples were annealed at 723 K for 1 h under ambient air. In this section, we did not produce any protective and conductive intermediate layer between Ti substrate and the active coating. To ensure the accuracy of the test data for the every electrode, all of the electrodes are repeatedly synthesized at least three times on the given hydrothermal conditions.

As a reference, the traditional RuO_2–TiO_2/Ti was also prepared via thermal decomposition of a mixture of $RuCl_3$ and tetrabutyl titanate dissolved in iso-propanol at 3:7 molar ratios. The Ti substrate was brushed with the precursors at room temperature, followed by drying at 373 K for 10 min to allow the solvent to vaporize, and then annealed at 723 K for 10 min. This procedure was repeated 10 times. Finally, the anode was annealed at 723 K for 1 h under ambient air.

2.2 Characterization and electrochemical measurements

The surface morphology and the microstructure of the catalysts were analyzed by X-ray diffraction (XRD-6000,

Shimadzu), field-emission scanning electron microscopy (FE-SEM, JSM-7800, Japan), and energy dispersive X-ray spectra (EDX, OXFORD Link-ISIS-300), respectively. Electrochemical measurements were conducted in a three-electrode cell system with an Electrochemical Workstation (Autolab electrochemical analyzer, PGSTAT302 N, Metrohm). The electrode area of the working electrode is 1 cm^2. A Pt foil in parallel orientation to the working electrode was used as the counter electrode and a saturated calomel electrode (SCE) as the reference electrode. Double layer capacitance of the electrodes was obtained by cyclic voltammetry (CV) at scan rate from 10 to 120 mV s^{-1}. And the catalytic performance of the prepared electrodes toward CER was systematically investigated in a 5 mol L^{-1} NaCl electrolyte (pH 3). The corrections for the IR-drop to the working electrode were made using electrochemical impedance spectroscopy (EIS) in the frequency range of 0.01 Hz–100 kHz.

3 Results and discussion

3.1 Surface morphology

FE-SEM analysis was performed to investigate the effect of the microstructure of prepared RuO_2–TiO_2/Ti anodes. For RuO_2–TiO_2/Ti obtained by the conventional thermal decomposition method, the surface of coating is typical mud-crack island-gap microstructure (denoted as MC-RuO_2–TiO_2/Ti, Fig. 1a). In contrast, three hydrothermal synthesized RuO_2–TiO_2/Ti anodes display completely different surface morphologies. Figure 1b shows that the nanoparticles RuO_2–TiO_2 are uniformly deposited onto the Ti substrate (denoted as NP-RuO_2–TiO_2/Ti). When increasing the concentration of hydrochloric acid from 0.5 to 1.0 wt%, the Ti substrate is well covered by the unique nano-flowerlike RuO_2–TiO_2 (denoted as NF-RuO_2–TiO_2/Ti, Fig. 1c). As the amount of hydrochloric acid further increased to 3.0 wt%, the surface morphology of the catalyst unexpectedly evolves into nano-rods (denoted as NR-RuO_2–TiO_2/Ti, Fig. 1d). Furthermore, the thickness of the three coating increases gradually with the increase of hydrochloric acid concentration (Fig. 2; Table 1), although it is hard to clearly distinguish the boundary between the coating and the substrate because they are directly grown onto the surface of the Ti substrate, rather than the formation under the thermal decomposition condition. The contents of titanium increase gradually with the increase of hydrochloric acid concentration, whereas the content of ruthenium shows an opposite trend through the EDX analysis. The traditional electrode obtained by thermal decomposition method still shows similar molar ratio of Ru/Ti to the initial stoichiometry. These obvious differences suggest that hydrochloric acid plays a critical role in regulating the catalyst size and morphology during the nucleation and growth process of RuO_2–TiO_2. We proposed the role of hydrochloric acid may be two-fold: one is to etch the Ti substrate to form titanium ions, which are easy to hydrolyze with water at the water/substrate interface, resulting in the slow oxidation process consuming dissolved oxygen to form a crystal nucleus on the substrate. After the formation of the first nanocrystalline layer, the deposition film is gradually formed with continuous hydrolysis and subsequent growth-crystallization. That is,

$$(Ru/Ti)^{3+} + H_2O \rightarrow (Ru/Ti)OH^{2+} + H^+;$$

$$(Ru/Ti)OH^{2+} + O_2 \rightarrow (Ru/Ti)(IV)\,\text{oxo species} + \text{species } O_2^- \rightarrow RuO_2/TiO_2$$

The acid condition could slow down the hydrolysis reaction of titanium ions by providing free H^+, which is necessary for the growth of depositions [29]. On the other hand, since the rutile (110) surface possesses the lowest energy [31] and has abundant five-fold coordinated titanium atoms, two-fold coordinated oxygen atoms and oxygen vacancies, it may be the favorite source of the selective adsorption of Cl^- on (110) plane and retard the growth rate of (110) surface [32, 33]. On the contrary, the other higher surface energy crystal surface can absorb more the Ti(IV) oxo species to decrease the surface energy. Thus, the crystal grows anisotropically along the (110) surface. With the extension of the hydrothermal reaction time, the crystal growth rate starts to decrease, and part of the crystals may begin to dissolve to form the Ti(IV) oxo species again. These species would diffuse to the solution and provide conditions for the random regrowth on the surface of the formed crystals. Accordingly, Cl^- adsorption plays a critical role in affecting the preferred crystal planes.

3.2 Microstructure

As the precursor materials prepared by the hydrothermal method do not show obvious diffraction peaks except the diffraction peaks of the Ti substrate, only the crystal structures of the RuO_2–TiO_2/Ti anodes after annealing treatment at 723 K for 1 h under ambient air were analyzed by XRD as shown in Fig. 3a. It can be seen that no peaks for pure rutile RuO_2 (PDF card No. 040-1290) and pure rutile TiO_2 (PDF card No. 021-1276) are observed in XRD patterns. The diffraction peaks at about 28° and 35.5° lie between the standard peaks of the pure RuO_2 and TiO_2 rutile phases. EDS analysis from Fig. 3b has also verified the presence of Ru, Ti and O in the representative NF-RuO_2–TiO_2/Ti. These results are almost consistent with that of previous literatures, namely, metal oxides are mainly present in the solid solution after annealing

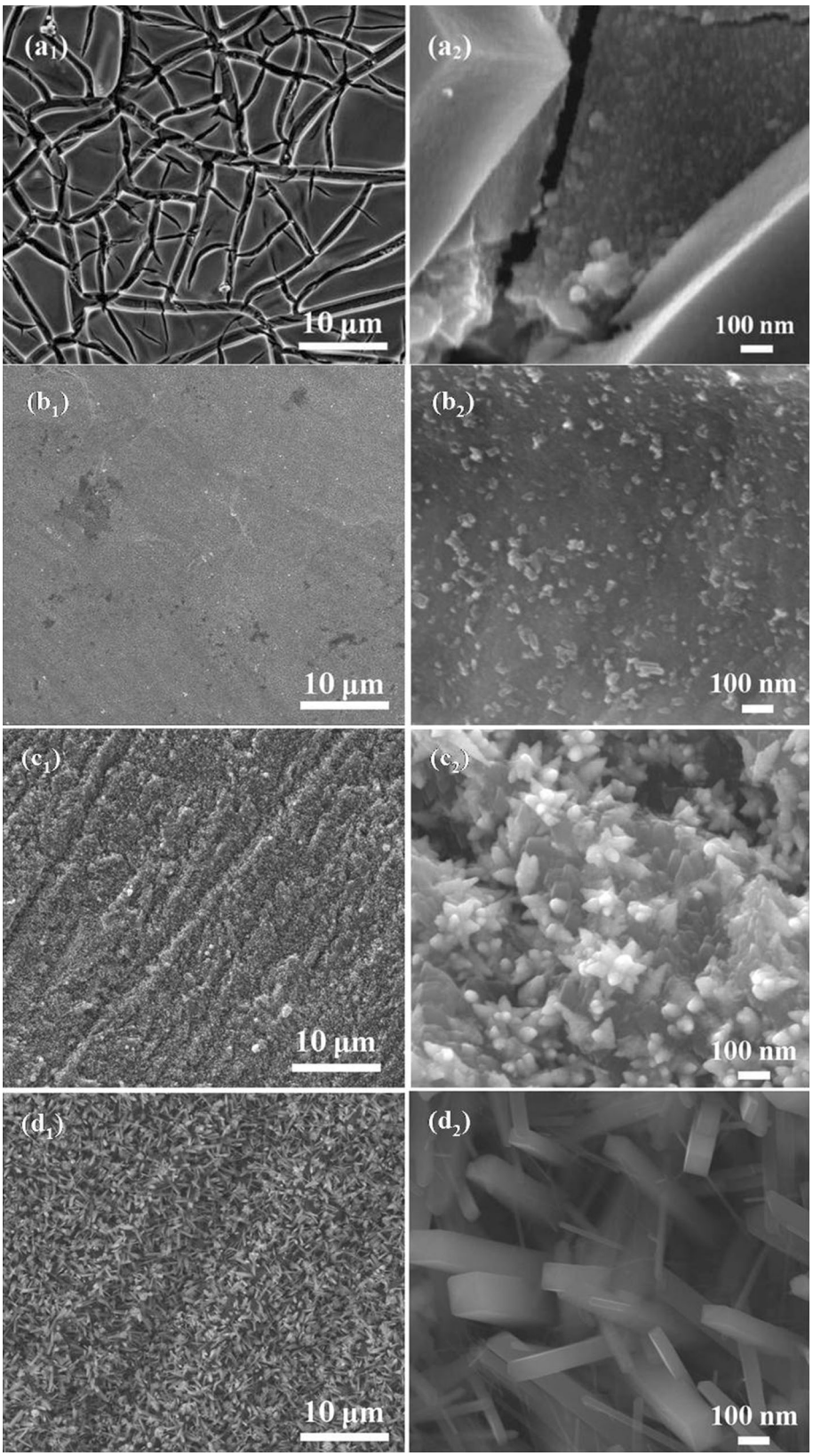

Fig. 1 FE-SEM images of $\mathbf{a}_1$, $\mathbf{a}_2$ MC-RuO_2–TiO_2/Ti; $\mathbf{b}_1$, $\mathbf{b}_2$ NP-RuO_2–TiO_2/Ti; $\mathbf{c}_1$, $\mathbf{c}_2$ NF-RuO_2–TiO_2/Ti; and $\mathbf{d}_1$, $\mathbf{d}_2$ NR-RuO_2–TiO_2/Ti anodes

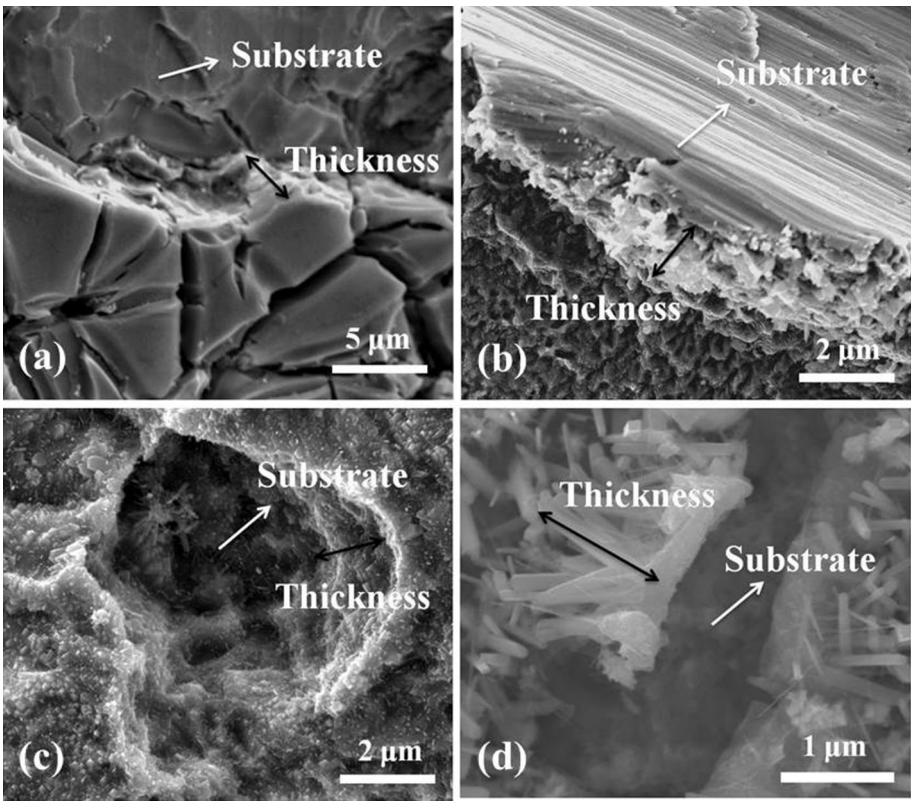

Fig. 2 The measurement of the coating thickness from FE-SEM images: **a** MC-RuO_2–TiO_2/Ti; **b** NP-RuO_2–TiO_2/Ti; **c** NF-RuO_2–TiO_2/Ti; and **d** NR-RuO_2–TiO_2/Ti anodes

Table 1 Chemical composition and thickness of the four coatings

Anodes	Atom (%)				Thickness (μm)
	Ru	Ti	O	Totals	
MC-RuO_2–TiO_2/Ti	11.37	25.91	62.72	100	2–3
NP-RuO_2–TiO_2/Ti	8.84	24.77	66.39	100	1–2
NF-RuO_2–TiO_2/Ti	8.10	26.22	65.68	100	1–2
NR-RuO_2–TiO_2/Ti	5.66	31.76	62.58	100	1–2

treatment at 723 K for 1 h under ambient air because they possess the same valence and similar ionic radius, satisfying the Hume-Rothery conditions for the formation of a solid solution [8, 34, 35]. Such formed solid solution catalyst shows a long-term stability because of the advantages of good electrical conductivity, excellent chemical stability and corrosion resistance in electrolysis [36, 37].

Moreover, we observed the difference from Fig. 3a that the intensity of diffraction peak of anatase TiO_2 at 25.58° (PDF card No. 021-1272) in RuO_2–TiO_2/Ti anodes gradually increases with increasing the concentration of hydrochloric acid during the hydrothermal process. When the concentration of hydrochloric acid reaches to 3.0 wt%, the intensity of anatase TiO_2 at 25.58° in NR-RuO_2–TiO_2/Ti obviously increases, whereas the intensities of rutile phase at 28.72° and 35.11° significantly decrease. This indicates that anatase TiO_2 has been the main component in NR-RuO_2–TiO_2/Ti anode, which is not desired in terms of the catalyst properties. Based on the EDX analysis over the high amount of Ti in NR-RuO_2–TiO_2/Ti from Table 1, the main reason is attributed to the surface of the Ti substrate seriously etched in 3.0 wt% hydrochloric acid under the hydrothermal conditions [38]. The formed titanium ions hydrolyze with water, turning to excess TiO_2 after annealing treatment at 723 K for 1 h under ambient air. Consequently, it is very important to choose appropriate concentration of hydrochloric acid for synthesizing RuO_2–TiO_2/Ti anode.

3.3 Electrocatalytic performance of CER for the anodes

To assess the catalytic activities of these three different morphology catalysts, the polarization curves for NP-RuO_2–TiO_2/Ti, NF-RuO_2–TiO_2/Ti and NR-RuO_2–TiO_2/Ti were performed in a 5 M NaCl electrolyte (pH 3). For

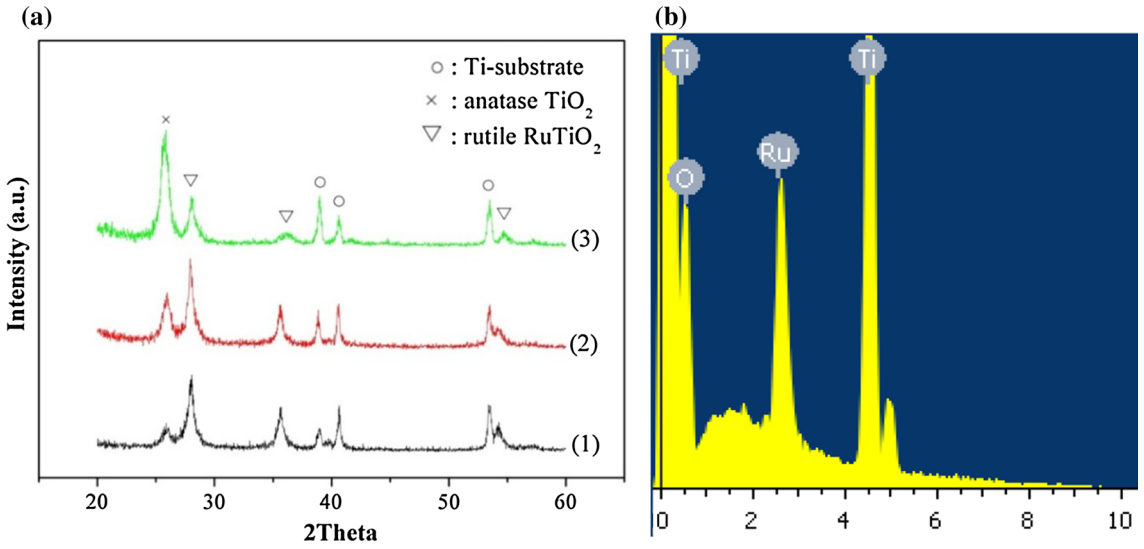

Fig. 3 **a** XRD patterns of (*1*) NP-RuO_2–TiO_2/Ti; (*2*) NF-RuO_2–TiO_2/Ti; and (*3*) NR-RuO_2–TiO_2/Ti anodes. **b** EDX analysis of representative NF-$RuTiO_2$/Ti anode

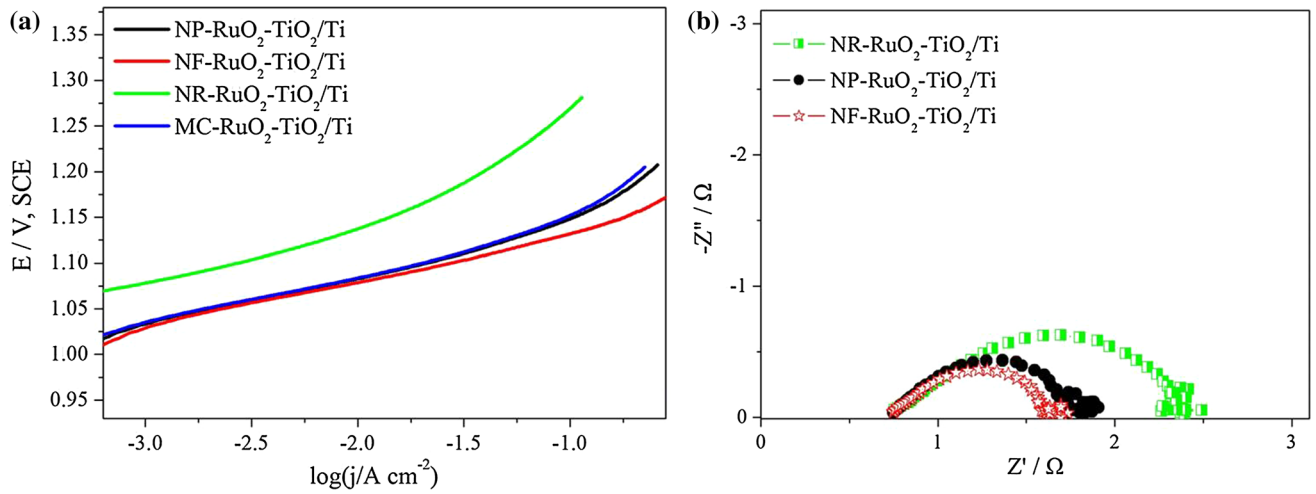

Fig. 4 **a** The polarization curves of the anodes with a sweep rate of 5 mV s^{-1} at room temperature; Electrolyte: 5 M NaCl, pH 3; The IR-drop was corrected; and **b** the corresponding Nyquist plots measured under galvanostatic mode, 20 mA cm^{-2}

comparison, the MC-RuO_2–TiO_2/Ti is also investigated under the same conditions. As depicted from Fig. 4a, the polarization curves of these catalysts show the typical shape of the CER, in which the current density obviously goes up with increasing sweep potentials. NF-RuO_2–TiO_2/Ti shows lower onset potential and more active than the other anodes under the identical conditions (Table 2) after the reaction is stable, indicating that it can catalyze CER at a significantly reduced electrode potential. The reason for NF-RuO_2–TiO_2/Ti with the highest catalytic activity toward CER is probably due to the unique surface structure that is beneficial for the interface reaction and diffusion of

Table 2 Electrochemical analysis of the anodes based polarization curves, CV in the double layer region and EIS curves

Anodes	$E^{[a]}_{conset}$ (V)	Tafel slopes	C_{dl} (μF cm^{-2})	Relative surface area	R_{ct} at 20 mA cm^{-2} (Ω cm^{-2})
NP-RuO_2–TiO_2/Ti	1.06	43	5620	281	1.02
NF-RuO_2–TiO_2/Ti	1.04	41	7480	374	0.87
NR-RuO_2–TiO_2/Ti	1.10	46	8360	418	1.61

[a]: The onset potential is defined as the potential at which the current density is 2 mA cm^{-2}

electrolyte and gas products. To estimate the electrochemical surface area of the prepared anodes, we measured CV responses and scan rate dependence of current densities for the anodes in the region of 0.6–0.8 V versus SCE (Fig. 5), which can be used as a classic method to determine the capacitance (C_{dl}) of the double layer at the solid/liquid interface of the electrode [39–42]. In this potential range, the main reaction is reversibly oxidized and reduced reaction between Ru (III) and Ru (IV). The current densities in the voltammograms increased with increasing the sweep rate. It appears from Table 2 that NF-RuO_2–TiO_2/Ti has a much larger C_{dl} than NP-RuO_2–TiO_2/Ti. Since C_{dl} is proportional to the electrochemical surface area, the results strongly suggest that the nano-flowerlike structure catalyst directly grown on the Ti substrate are more effective in enlarging the catalytically active surface area as compared to conventional planar catalyst films coated on electrodes. Accordingly, better exposure and enhanced utilization of electroactive sites (e.g. Ru species) on the large active surface of NF-RuO_2–TiO_2/Ti greatly contribute to its CER activity. However, the surface area is not the only factor that contributes to the activity. For example, the relative surface area of NF-RuO_2–TiO_2/Ti is smaller than that of NR-RuO_2–TiO_2/Ti. That is to say, the trend of the relative surface area for both NF-$RuTiO_2$/Ti and NR-$RuTiO_2$/Ti is inconsistent with their activity. Considering the slight differences over the Tafel slope of the CER for the catalysts, it suggests that the reaction mechanism is not changed. In this case, we guess the polarization resistance of the electrode might be the main factor for influencing the catalytic activity of the electrode. The electrochemical impedance spectroscopy (EIS) analysis is thus employed to further investigate the activity of the electrodes. The charge transfer resistance (R_{ct}) is an indicator highly related to the electrocatalytic behavior: the lower R_{ct} value, the better activity for the catalysis of CER [43, 44]. The Nyquist plots of the electrodes as shown in Fig. 4b reveals that the R_{ct} of NF-RuO_2–TiO_2/Ti is lower than those of NP-RuO_2–TiO_2/Ti and NR-RuO_2–TiO_2/Ti. The NR-RuO_2–TiO_2/Ti electrode possesses the highest R_{ct} value because of high amount of TiO_2 in catalyst based on the results of the EDX and XRD analysis, which is consistent with its poor activity for CER. Therefore, NF-RuO_2–TiO_2/Ti is the best one for catalysis of the CER in the studied electrodes.

As aforementioned in the activity test, NF-RuO_2–TiO_2/Ti with a nano-flowerlike structure displays superior activity for CER compared to the other two morphology anodes. NF-RuO_2–TiO_2/Ti is therefore selected as a typical object to determine its activity and stability. For purpose of comparison, the catalytic activity and stability of the traditional MC-RuO_2–TiO_2/Ti prepared via thermal decomposition method is also investigated at the same condition. It can be seen from the results in Fig. 6a, NF-RuO_2–TiO_2/Ti has better activity for CER than MC-RuO_2–TiO_2/Ti. After 1200 min electrolysis, the polarization curve of NF-RuO_2–TiO_2/Ti shows negligible difference compared with the initial one. Moreover, it shows almost constant potential during the electrolysis (Fig. 6b). In sharp contrast, the catalytic activity of traditional MC-RuO_2–TiO_2/Ti seems to degrade significantly compared to the initial one. And the voltage is also further increased as a function of electrolysis time. These results suggest that NF-RuO_2–TiO_2/Ti possesses superior stability in the electrochemical process. There are two main factors that are thought to be responsible for the superior stability of NF-RuO_2–TiO_2/Ti. First, the integration of RuO_2–TiO_2 coating on the Ti substrate without obvious crack by hydrothermal technology might display good mechanical adhesion between the coating and

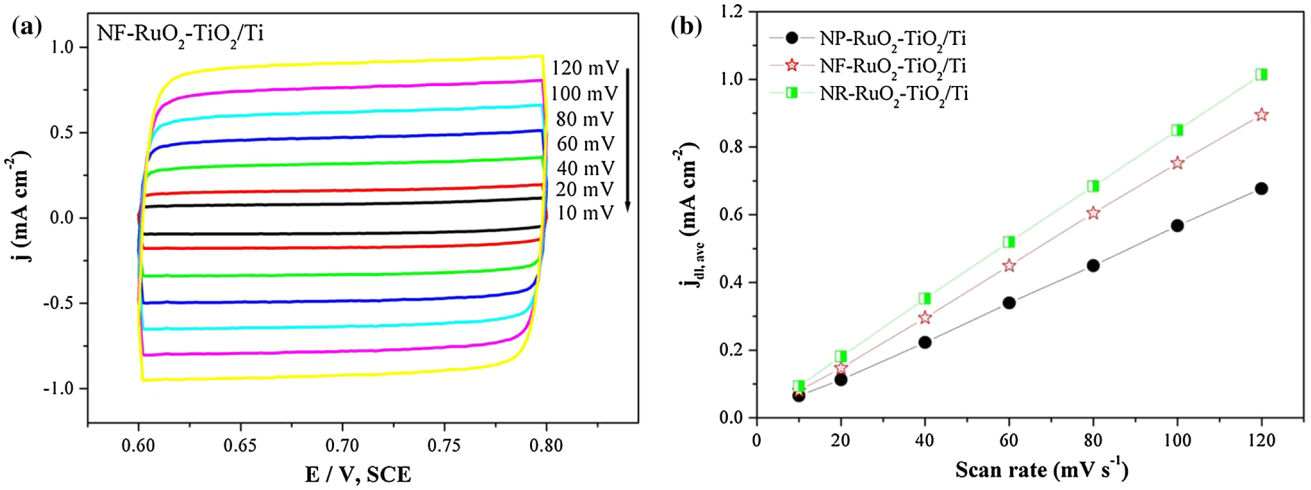

Fig. 5 **a** CV of the representative NF-RuO_2–TiO_2/Ti at different scan rate in the double layer region; and **b** the current density at 0.7 V vs. SCE plotted against scan rate fitted to a linear regression allows for the estimation of C_{dl}

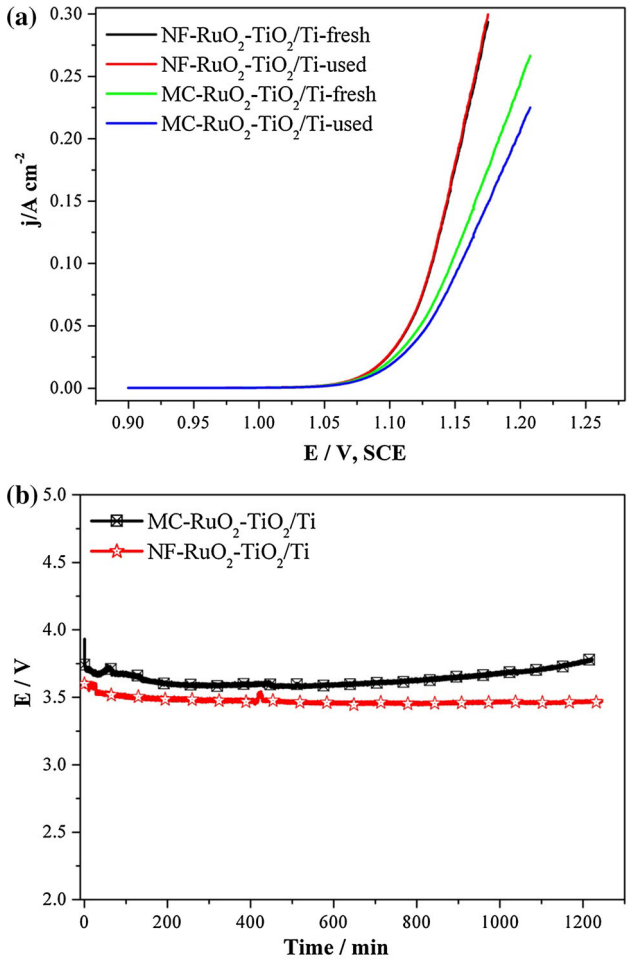

Fig. 6 **a** The polarization curves of NF-RuO_2–TiO_2/Ti initially and after 1200 min electrolysis in a 5 mol L^{-1} NaCl electrolyte (pH 3); The IR-drop was corrected; and **b** the corresponding time-dependent potential curves under a constant anodic current density of 1.0 A cm^{-2} for 1200 min

the substrate. Second, the nano-flowerlike RuO_2–TiO_2 with outstretched structure is beneficial for increasing the surface area, the diffusion of electrolyte and the disengagement of gas bubbles. Lu and co-workers have shown that MoS_2 arrays possess a smaller bubble adhesion force underwater than a flat electrode, and that the gas bubble naturally left the surface with ease at the end [45]. Accordingly, the stable architecture ensures that the NF-RuO_2–TiO_2/Ti works for a long-term during the whole electrolysis process.

4 Conclusions

In summary, the nanostructured RuO_2–TiO_2 anodes with different surface morphologies have been grown in situ onto the surface of Ti substrate by hydrothermal treatment for the first time. In this process, hydrochloric acid plays an important role in the formation of different surface morphologies. The etched Ti^{3+} and Ru^{3+} are easy to hydrolyze with water at the water/substrate interface, resulting in the slow oxidation process consuming dissolved oxygen to form a crystal nucleus on the substrate. After the formation of the first nanocrystalline layer, the deposition film is gradually formed with continuous hydrolysis and subsequent growth-crystallization. The resultant NF-RuO_2–TiO_2/Ti after annealing treatment exhibited good catalytic performance for CER because of the low R_{ct} and high surface area. This work may open up a new route toward designing coating electrode with controllable structure for electrolytic applications.

Acknowledgments This research work was financially sponsored by National Basic Research Program of China (Grant No.: 2012CB720300), by National Natural Science Foundation of China (Grant Nos.: 21306232, 51072239, and 21376284).

References

1. Fauvarque J (1996) The chlorine industry. Pure Appl Chem 68:1713–1720
2. Trasatti S (2000) Electrocatalysis: understanding the success of DSA. Electrochim Acta 45:2377–2385
3. Over H (2013) Atomic scale insights into electrochemical versus gas phase oxidation of HCl over RuO_2-based catalysts: a comparative review. Electrochim Acta 93:314–333
4. Xiong K, Li L, Deng ZH, Xia MR, Chen SG, Tan SY, Peng XJ, Duan CY, Wei ZD (2012) RuO_2 loaded into porous Ni as a synergistic catalyst for hydrogen production. RSC Adv 4:20521–20526
5. Moussallem I, Jorissen J, Kunz U, Pinnow S, Turek T (2008) Chlor-alkali electrolysis with oxygen depolarized cathodes: history, present status and future prospects. J Appl Electrochem 38:1177–1194
6. Beer HB (1965) Improvements in or relating to electrodes for electrolysis. British Patent, p 10
7. Comninellis C, Vercesi GP (1991) Problems in DSA® coating deposition by thermal decomposition. J Appl Electrochem 21:136–142
8. Gaudet J, Tavares AC, Trasatti S, Guay D (2005) Physicochemical characterization of mixed RuO_2-SnO_2 solid solutions. Chem Mater 17:1570–1579
9. Lian F, Xin YL, Ma BJ, Xu LK (2015) Effect of carbon nanotubes on anodic properties of Ti/Ru-Ir-Sn oxides. J Electrochem 21:357–381
10. Ji L, Wang JT, Liu WB, Xue GL (2008) The effect of Ru: Sn on properties of Ru-Ir-Sn oxide anode coatings. J Electrochem 14:263–268
11. Petrykina V, Macounová K, Okubea M, Mukerjee S, Krtil P (2013) Local structure of Co doped RuO_2 nanocrystalline electrocatalytic materials for chlorine and oxygen evolution. Catal Today 202:63–69
12. Xiong K, Deng ZH, Li L, Chen SG, Xia MR, Zhang L, Qi XQ, Ding W, Tan SY, Wei ZD (2013) Sn and Sb co-doped RuTi oxides supported on TiO_2 nanotubes anode for selectivity toward electrocatalytic chlorine evolution. J Appl Electrochem 43:847–854

13. Takasu Y, Sugimoto W, Nishiki Y, Nakamatsu S (2010) Structural analyses of RuO_2-TiO_2/Ti and IrO_2-RuO_2-TiO_2/Ti anodes used in industrial chlor-alkali membrane processes. J Appl Electrochem 40:1789–1795
14. Wang QQ, Liu GC (2005) Progress in study on the mechanism of ruthenium –titanium anode. Chlor-Alkali Industry 12:20–27
15. Hansen HA, Man IC, Studt F, Abild-Pedersen F, Bligaard T, Rossmeisl J (2010) Electrochemical chlorine evolution at rutile oxide (110) surfaces. Phys Chem Chem Phys 12:283–290
16. Exner KS, Anton J, Jacob T, Over H (2014) Controlling selectivity in the chlorine evolution reaction over RuO_2-based catalysts. Angew Chem Int Edit 53:11032–11035
17. Karisson RKB, Hansen HA, Bligaard T, Cornell A, Pettersson LGM (2014) Ti atoms in $Ru_{0.3}Ti_{0.7}O_2$ mixed oxides form active and selective sites for electrochemical chlorine evolution. Electrochim Acta 146:733–740
18. Profeti D, Lassali TAF, Olivi P (2006) Preparation of $Ir_{0.3}Sn_{(0.7-x)}Ti_xO_2$ electrodes by the polymeric precursor method: characterization and lifetime study. J Appl Electrochem 36:883–888
19. Liang CH, Jia LN, Huang NB (2012) Preparation of Ru-Ir-Sn-Ti metal oxide anode coating by sol-gel method and study on its electrochemical properties. Surf Tech 41:26–29
20. Panic VV, Dekanski AB, Mitric M, Milonjic SK, Miskovic-Stankovic VB, Nikolic BZ (2010) The effect of the addition of colloidal iridium oxide into sol-gel obtained titanium and ruthenium oxide coatings on titanium on their electrochemical properties. Phys Chem Chem Phys 12:7521–7528
21. Seifollahi M, Jafarzadeh K (2009) Stability and morphology of $(Ti_{0.1}Ru_{0.2}Sn_{0.7})O_2$ coating on Ti in chlorakali medium. Corros Eng Sci Techn 44:362–368
22. Trieu V, Schley B, Natter H, Kintrup J, Bulan A, Hempelmann B (2012) RuO_2-based anodes with tailored surface morphology for improved chlorine electro-activity. Electrochim Acta 78:188–194
23. Krishtalik LI (1981) Kinetics and mechanism of anodic chlorine and oxygen evolution reactions on transition metal oxide electrodes. Electrochim Acta 26:329–337
24. Fernandez JL, de Chialvo MRG, Chialvo AC (2000) AC analysis of the Volmer-Krishtalic mechanism for the chlorine electrode reaction. Electrochem Commun 2:630–635
25. Thomassen M, Karlsen C, Borresen B, Tunold R (2006) Kinetic investigation of the chlorine reduction reaction on electrochemically oxidised ruthenium. Electrochim Acta 51:2909–2918
26. Bavykin DV, Friedrich JM, Walsh FC (2006) Protonated titanates and TiO_2 nanostructured materials: synthesis, properties, and applications. Adv Mater 18:2807–2824
27. Ye M, Liu HY, Lin C, Lin Z (2013) Hierarchical rutile TiO_2 flower cluster-based high efficiency dye-sensitized solar cells via direct hydrothermal growth on conducting substrates. Small 9:312–321
28. Ding R, Qi L, Jia M, Wang H (2013) Hydrothermal and soft-templating synthesis of mesoporous $NiCo_2O_4$nanomaterials for high-performance electrochemical capacitors. J Appl Electrochem 43:903–910
29. Cai J, Ye J, Chen S, Zhao X, Zhang D, Chen S, Ma Y, Jin S, Qi L (2012) Self-cleaning, broadband and quasi-omnidirectional antireflective structures based on mesocrystalline rutile TiO_2 nanorod arrays. Energ Environ Sci 5:7575–7581
30. Qu Y, Zhou W, Ren ZY, Wang GF, Jiang BJ, Fu HG (2014) Facile synthesis of porous $Zn_2Ti_3O_8$ nanorods for photocatalytic overall water splitting. ChemCatChem 6:2258–2262
31. Oliver PM, Watson GW, Kelsey ET, Parker SC (1997) Atomistic simulation of the surface structure of the TiO_2 polymorphs rutile and anatase. J Mater Chem 7:563–568
32. Huang Q, Gao L (2003) A simple route for the synthesis of rutile TiO_2 nanorods. Chem Lett 32:638–639
33. Hosono E, Fujihara S, Kakiuchi K, Imai H (2004) Growth of submicrometer-scale rectangular parallelepiped rutile TiO_2 films in aqueous $TiCl_3$ solutions under hydrothermal conditions. J Am Chem Soc 126:7790–7791
34. Kong HS, Lu HY, Zhang WL, Lin HB, Huang WM (2012) Performance characterization of Ti substrate lead dioxide electrode with different solid solution interlayers. J Mater Sci 47:6709–6715
35. Malek J, Watanabe A, Mitsuhashi T (2000) Sol-gel preparation of rutile type solid solution in TiO_2-RuO_2 system. J Therm Anal Calorim 60:699–705
36. Jovanovic VM, Dekanski A, Despotov P, Nikolic BZ, Atanasoski RT (1992) The roles of the ruthenium concentration profile, the stabilizing component and the substrate on the stability of oxide coatings. J Electroanal Chem 339:147–165
37. Evdokimov SV (2002) Electrochemical and corrosion behavior of electrode materials based on compositions of ruthenium dioxide and base-metal oxides. Russ J Electrochem 38:583–588
38. Allam NK, Grimes CA (2007) Formation of vertically oriented TiO_2 nanotube arrays using a fluoride free HCl aqueous electrolyte. J Phys Chem C 111:13028–13032
39. Trasatti S, Petrii OA (1992) Real surface area measurements in electrochemistry. J Electroanal Chem 327:353–376
40. Zhang L, Xiong K, Chen SG, Li L, Deng ZH, Wei ZD (2015) In situ growth of ruthenium oxide-nickel oxide nanorod arrays on nickel foam as a binder-free integrated cathode for hydrogen evolution. J Power Sources 274:114–120
41. Ma TY, Dai S, Jaroniec M, Qiao SZ (2014) Metal-organic framework derived hybrid Co_3O_4-carbon porous nanowire arrays as reversible oxygen evolution electrodes. J Am Chem Soc 136:13925–13931
42. Pu ZH, Liu Q, Asiri AM, Sun XP (2014) Ni nanoparticles-graphene hybrid film: one-step electrodeposition preparation and application as highly efficient oxygen evolution reaction electrocatalyst. J Appl Electrochem 44:1165–1170
43. Alves VA, da Silva LA, Boodts JFC (1998) Electrochemical impedance spectroscopic study of dimensionally stable anode corrosion. J Appl Electrochem 28:899–905
44. Gao J, Zhu Y, Ren Z, Li W, Quan S, Liu Y, Wang Y, Chai B (2015) Electrocatalytic performance of $Ir_{0.5}Pt_{0.5}O_2$ anode and preparation of electrolyzed oxidizing water. CIESC J 66: 992–1000
45. Lu ZY, Zhu W, Yu XY, Zhang HC, Li YJ, Sun XM, Wang XW, Wang H, Wang JM, Luo J, Lei XD, Jiang L (2014) Ultrahigh hydrogen evolution performance of under-water "Superaerophobic" MoS_2 nanostructured electrodes. Adv Mater 26:2683–2687